Experimental investigation on the effect of micropitting on friction - Part 2: Analysis of power losses evolution on a geared system

T. Touret, C. Changenet, F. Ville, J. Cavoret

Experimental investigation on the effect of micropitting on friction - Part 2: analysis of power losses evolution on a geared system

T. TOURET[a,*], C. CHANGENET[a], F. VILLE[b], J. CAVORET[b]

[a] *Univ Lyon, ECAM Lyon, INSA-Lyon, LabECAM, F-69005 Lyon, France*
[b] *Univ Lyon, INSA-Lyon, CNRS UMR5259, LaMCoS, F-69621 Villeurbanne, France*

Abstract

In this paper, an experimental investigation on a FZG test rig is presented. The proposed approach aims to at highlight the influence of micropitting on power losses and temperatures in this geared system. Micropitting has been gradually developed on the gear pair by applying increasing load levels. The influence of this defect on power losses and temperatures has been evaluated with specific characterisation tests performed alongside micropitting growth. The modification of the gear surface roughness was monitored during these tests. This study shows power loss and oil temperature increase due to micropitting development. Furthermore, it is possible to correlate power loss and temperature variations to surface feature measurements.

Keywords: , FZG test rig, Micropitting, Gearbox, Diagnostics, experiments

1. Introduction

Industry aims to optimise mechanical systems by increasing speed and reducing size. As a consequence, these systems operate under more severe conditions which may generate more frequent and complex failures of main mechanical components, -i.e.: gears and rolling elements bearings. Hence condition monitoring (CM) received a growing interest in recent years. Vibration or acoustic

*Corresponding author
URL: thomas.touret@ecam.fr (T. TOURET)

based methods are the most commonly used approaches to investigate failure in geared systems whether in the area of scientific literature [1] or industry [2]. Yet, extracting information from the noisy signal and identifying the fault signature are challenging due to the large number of vibration sources emitting simultaneously in a geared system. Hence, alternative methods are being investigated such as transmission error analyses [3], oil contamination analyses [4] or electric spectrum analyses [5] (when gearbox is coupled with an electric motor). Another possible approach consists in studying gearbox temperature variations due to faults. This approach is getting an increasing interest in the past years [6] showing temperature could be a reliable indicator. Indeed temperature may constitute an attractive alternative compared to vibrational or acoustic analysis as sensors are less expensive, reliable and are able to measure an array or a localised temperature according to the needs of the study. Most of the investigated failures consist in large mechanical defects, such as spalling or tooth rupture, which generate specific temperature variation up to a dozen degrees in some applications [6]. Smaller defects such as micropitting, were not investigated in the reviewed studies. Yet this kind of defect, which is not critical in several cases, may also degenerate into a larger defect [7, 8]. Furthermore, micropitting is difficult to predict [9, 10], as it strongly depends on operating conditions [11, 12], surface features [13], material thermochemical treatment [14, 15] or oil and its composition [16, 17]. For all these reasons developing a CM method to detect micropitting could be relevant. This study focuses on the influence of micropitting on power losses and temperatures in a geared system. Power losses are investigated as they are proportional to the friction coefficient in the gear contact and should be significantly impacted by micropitting. This paper follows a first work [18] where the link between micropitting and friction was experimentally measured using a tribo-meter and contact conditions were controlled. The first section of the paper summarizes these above mentioned results. The second one presents the proposed methodology. In a third part, the experimental results regarding power losses are shown and analysed. The relationship between the evolution of power losses and oil temperature is also

highlighted. Finally, the last part proposes some conclusions on the effect of micropitting on friction.

2. Summary of previous results

To investigate the influence of micropitting on power losses and temperatures, it was assumed that micropitting is able to modify enough gear surface features to increase friction coefficient. This could imply an increase of the power losses, that could, ultimately, generate a temperatures increase as presented in Figure 1.

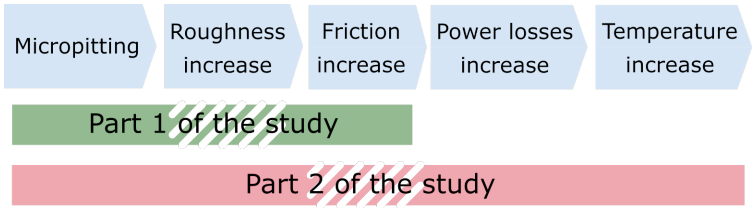

Figure 1: Decomposition of the study between part 1 [18] and part 2

The study was decomposed into two parts as presented in Figure 1. The first part of this investigation was published in a previous paper [18] which focused on investigating the link between micropitting and friction coefficient using a tribometer. This apparatus allowed to simulate gear contact condition by controlling slide to roll ratio, contact pressure and surface velocity of two rotating discs. This study underlines a clear dependency between the amount of micropitts on the surface and the friction coefficient as reported in Figure 2.

The second part of this investigation, presented in this paper, aims at extending these observations to a geared system. To this end, the influence of micropitting on power losses has to be studied, as well as temperature sensitivity in order to validate its correlation with power losses.

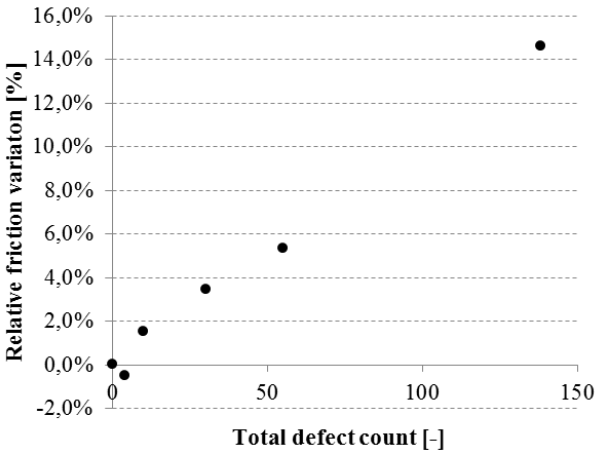

Figure 2: Correlation between friction coefficient and defect count measured in part 1 [18]

3. Methodology

A back-to-back FZG test rig was used in this study (see figure 3). It is composed of two gearboxes in a closed mechanical loop. The test gearbox is equipped with type C standard gears (described in Table 2).Detailed Gear description can be found in [19] . Gear set is splash lubricated with commercial 85W90 oil whose properties are given in Table 1. A HBM T22 torque meter is used to measure the resistive torque generated in the system. Type K thermo-couples are placed in the oil sump and outside of the gearbox in order to measure air temperature. Only the test gearbox will suffer micropitting during the fatigue tests.

Measuring friction in the contact of a geared system is challenging, especially in a closed mechanical loop such as the FZG test rig. Evolution of the friction generated at the gear contact over the test will be measured through the evolution of the total resistive torque. Power losses are directly derived from torque measurements as the rotating speed is controlled. To study the correlation between micropitting and the variations of power losses, or temperatures, successive steps will be performed in order to induce a progressive increase of the micropitted surface. Each step is composed of three phases as (Figure 4):

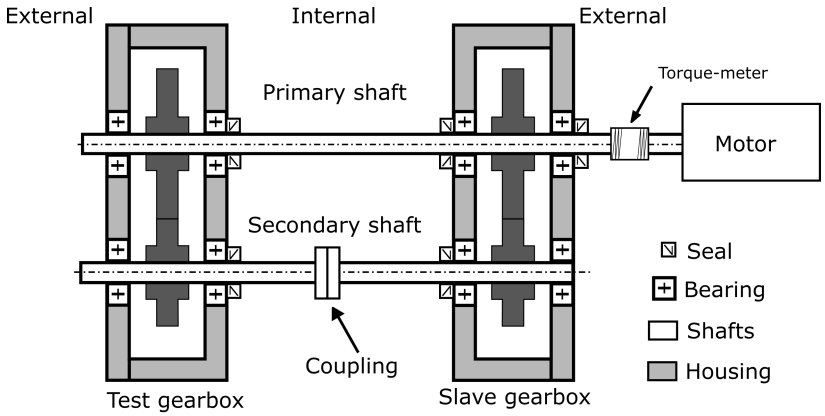

Figure 3: Cross section representation of the FZG test rig

1. **Fatigue** phase is firstly performed to develop micropitting magnitude on gear flanks. This phase is done by changing operating condition as described in 3.1.
2. **Metrology** phase is then performed to observe and measure gear surface evolution as described in section 3.2
3. **Caracterisation** phase is performed to measure power losses variation in repeatable operating condition as described in section 3.3.

In addition with each complete step, an initial step is performed without fatigue phase in order to have a reference starting point. This test will be referred as "Step 0" here after. Operating condition of this step is the same as the other ones and is described in Table 4

Oil properties		
Reference	Fuchs Titan Gear HYP SAE 85W90	
Density	885	[kg / m^3]
Kinematic viscosity @40	180	[mm^2 /s]
Kinematic viscosity @100	16.5	[mm^2/s]

Table 1: Oil properties

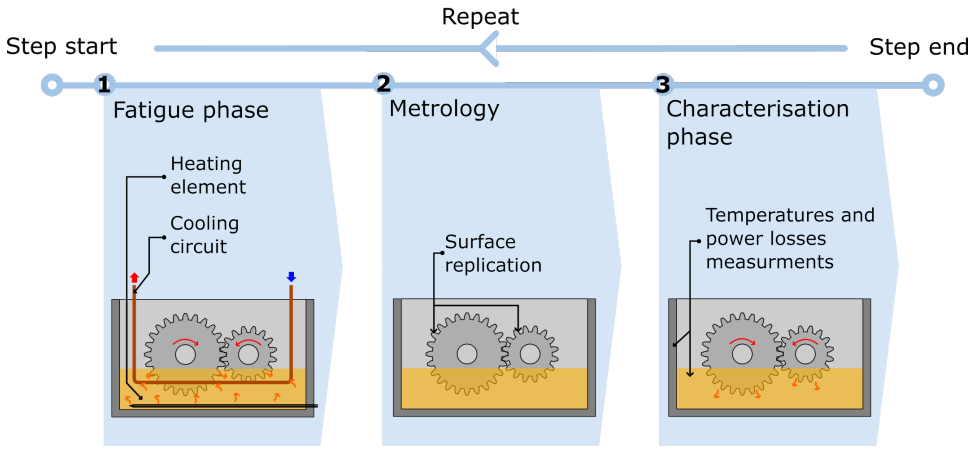

Figure 4: General experimental approach

Type C Gear set

Dimension	Symbol	Pinion Value	Wheel Value	Unit
Operating Center distance	a	91.5		[mm]
Tooth width	b	14.0		[mm]
Module	m	4.5		[mm]
Number of teeth	Z_i	16	24	[-]
Profile shift modification	X_i	0.1817	0.1715	[-]
Pressure angle	α	20		[deg]
Contact ratio	ε_α	1.46		[-]
Surface roughness	R_a	0.5		[µm]

Table 2: FZG Type C Gear definition

3.1. Fatigue phase

The FZG test rig was originally designed to compare the protective effect of a given lubricant on gear surface failure. The procedure is normalized with operating conditions and gear sets to qualify oil protection against pitting, micropitting, scuffing and wear. The aim of this study is to generate only micropitting on tooth gear surface. Therefore normalized micropitting procedure was used as reference.

Oil bath temperature is controlled during the fatigue phase. An heating element and cooling circuit allow to maintain an operating temperature close to

80°C.

Because of the loading mechanism, a limited set of torque is possible.

The proposed approach is based on the reference procedures which describe the operating conditions in order to generate micropitting. One "long procedure" [20] is associated with a transmitted torque which gradually increases by using all possible levels from $84N.m$ to $372N.m$. One "short procedure" [19] uses only two loading stages at $183N.m$ and $302N.m$. All stages are performed at the same speed during 2.16 million cycles. Literature [21, 22, 23, 24, 10] tends to modify slightly this procedure by reducing the fatigue duration to 1.44 million cycles and changing step count and loading.

In this study, operating conditions are chosen in order to ensure maximum discretization of the micropitting growth. To this end a preliminary fatigue test was performed to adjust them. This preliminary test showed, for example, that reducing the test duration to 4h was sufficient in order to obtain micropitting. This represents 0.72 million fatigue cycles for each step (on the wheel side). The same test also showed that load stage 9 generates significantly more wear than micropitting. So, unlike in the literature, the maximum loading used in this study was limited to load stage 8 ($239.3N.m$ on the pinion). The last fatigue step was doubled (Step 3-b) in order to obtain another fatigue step without increasing load. Experimental conditions are given in Table 3.

[1] This oil volume correspond to an oil level located 15mm below the shaft axis.

Step	1	2	3	3-b
Loading stage	L5	L7	L8	L8
Pinion torque [N.m]	94.1	183.4	239.3	239.3
Wheel rotational speed [rpm]	2000			
Transmitted Power [kW]	26.4	57.6	75.2	75.2
Oil volume[1] **[l]**	1.5			
Fatigue Cycles [-]	0.72 million			
Lambda ratio [-]	1.70	1.52	1.45	1.45

Table 3: Operating conditions during the micropitting phase

3.2. Surface Metrology

The metrology phase is performed to provide representative surface feature parameters of the surface evolution due to micropitting. Two types of indicators are measured:

- The "micropitted surface area" quantifies the ratio between the tooth surface area that presents dense micropitting compared to the total operating one.
- Surface roughness parameters are measured for three different tooth areas: at the tip, near the center and at the root of gear tooth. Surface quadratic roughness amplitude S_q and quadratic slopes S_{dq} are calculated from surface measurements. These parameters are classically used to estimate the roughness influence on friction coefficient [25, 26, 27]. These two parameters allow to quantify the surface aspect. As an example, for identical value of S_q, higher value of S_dq means a "sharper" roughness which is

correlated to its wavelength.

Surface feature measurements are performed on a replication of the gear tooth surface by using a specific resin and an optical interferometer. The procedure is described bellow:

1. Test rig cover is removed, the desired tooth is identified.
2. Tooth surface is cleaned from all residual lubricant.
3. The resin is applied on the tooth as shown in Figure 5.
4. Once this replication is hardened, it is removed and can be used on the microscope.

Figure 5: Replication resin on the tooth flank inside the test rig

This method has to be used in order to measure precisely surface roughness: interferometer microscope must be orthogonal and very close (2-3 mm) to the surface to obtain a correct measurement. With this method, surface features can be measured with a resolution of $0.001 \mu m$

3.3. Characterization phase

Characterization tests are performed in order to quantify the influence of micropitting growth on power losses and temperatures. In this phase, load stage

4 is chosen because this torque level is not expected to generate micropitting [24]. Operating condition used for the characterisation phase is reported in Table 4.

Loading stage	**Pinion torque [N.m]**	**Wheel rotating speed [rpm]**
L4	60.8	2000
Transmitted Power [kW]	**Oil Volume[1] [l]**	**Oil temperature [°C]**
19.1	1.5	80

Table 4: Operating condition in the characterization phase

It has been shown in the first part of the study [18] that micropitting can increase gear tooth friction by 10 %. Friction coefficient has a direct influence on gear power losses has shown by the ISO TR 14179-2 expression [28]:

$$P_{Gear} = f P_{in} H_v \tag{1}$$

Where f represents the average friction coefficient, P_{in} is the input power and H_v is a tooth geometry parameter.

Friction coefficient, f, is expected to evolve with surface roughness. Depending on the considered relationship, various parameters may be used. Schlenk equation from ISO TR 14179-2 [28] considers the arithmetic roughness R_a as representative of the roughness. Kelley-Lemanski [29] equation uses the quadratic roughness R_q parameter. Another law proposed by Diab *et al.* [30] uses both a parameter derived from the quadratic roughness and the quadratic roughness slope parameter R_dq.

The power losses that are determined with the resistive torque are the sum of all the power losses generated in both the test and slave gearboxes. In each gearbox, power losses are generated by the components as described in the ISO TR 14179-2 [28] and reported in equation 2:

$$P_{Total} = [P_{Gear,Friction} + P_{Gear,Hydraulic} + P_{Bearing} + P_{Seal}]_{Test,Slave} \tag{2}$$

Where $P_{Gear,Friction}$ represents gear Friction power losses, $P_{Gear,Hydraulic}$ is gear dissipation associated with splash lubrication, $P_{Bearing}$ represents bearing power losses and P_{Seal} the ones associated with seals.

The ISO TR 14179-2 [28] also shows that the relationship between power losses and oil temperature can be estimated from equation:

$$T_{Oil} = T_{Air} + \frac{P_{Gearbox}}{kA_{housing}} \tag{3}$$

Where T_{Oil} and T_{Air} represent respectively oil and air temperatures, $P_{Gearbox}$ is the total gearbox power losses, k an overall heat exchange coefficient and $A_{housing}$ the heat exchange area. This formulation underlines the correlation between total power losses and oil sump temperature. Yet the temperature sensitivity to the variation of a single source of power losses still has to be quantified.

As temperature has an impact on power losses [31], thermal management is crucial in order to obtain similar experimental conditions. The experimental procedure follows the methodology described thereafter in order to overcome this issue: no temperature regulation is set up during the characterisation tests, as it will hide small temperature variation due to power loss alterations. Tests are started with the test rig at ambient temperature. The room is isolated from any air conditioning system.

4. Experimental results

4.1. Power loss evolution analyses

Two successive characterisation tests (Step 0) were performed in order to validate the repeatability of the proposed approach. The associated power losses measurements are reported in figure 6.

This figure validates the repeatability of the approach and also shows the evolution of power losses during a characterisation test. First power losses strongly reduce due to viscosity decrease caused by temperature accommodation. Then

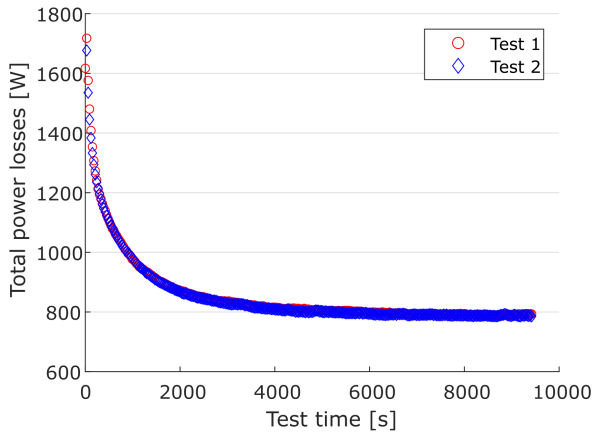

Figure 6: Evolution of the measured power losses during two characterization tests

these parameters stabilise when machine thermal equilibrium is reached. During test 1, oil sump temperature reaches 52.7 °C above the one of the room, and 53.2 °C during test 2. Similar measurements were obtained for each step. To compare steps together, power losses are averaged by using 10 minutes of data starting from the 110th minute (6600th second) since the beginning of each test. This starting point was chosen in order to consider corresponds to a time interval where torque was constant for all steps.

Along all steps, this approach results in the power loss variations reported on Figure 7.

Various tendencies can be observed with this test:

- **From Step 0 to Step 1**: Measured power losses decrease to a minimum value.
- **Between Steps 1 and 3**: Power losses increase.
- **Between Steps 3 and 3b**: Power losses tend to stabilize.

Torque changes in a range of $0.25 N.m$ that represents a power loss variation of 60W. These evolutions must be discussed regarding torque measurement accuracy.

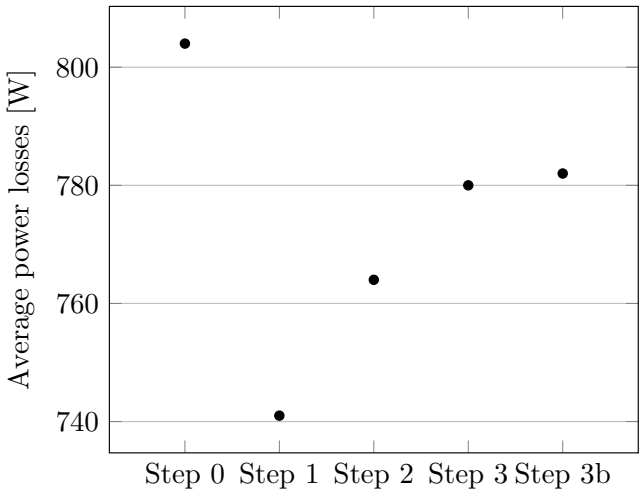

Figure 7: Evolution of the measured total power losses at each step

Discussion on torque measurement reliability

The torque meter used during tests has a full scale range of $50N.m$. It is a class 0.5 sensor, meaning that the total measurement uncertainty is estimated as $0.5/100 * FullScale$, in other words $0.25N.m$. It appears significant compared to the actual measured variation. Yet, this uncertainty includes the sensor thermal drift, the systematic error (measurement offset), the measurement noise and the linear error. To ensure good measurement repeatability, thermal drift is taken into account by compensating air temperature. Measurement noise is reduced by, first, having raw data averaged for 30s on the data logger and, secondly, by re-averaging the data on a 10 min interval. The systematic error is avoided as only relative variations are studied. Only the linear error is not compensated but can be neglected as it depends on the measurement variation, which is limited in this test. Considering these observations, the measured power loss variations are non negligible and clearly show that the fatigue test results in a measurable alteration of the test rig efficiency.

4.2. Micropitting and surface analyses

Surface evolution was observed on two specific teeth along the steps: one tooth from the wheel and one from the pinion. Surface pictures used to estimate micropitted area are compiled from four pictures as the tooth is too large to be observed from a single microscope observation. As an example, Figure 8 shows the wheel tooth surface after stage 3. Surface with dense micropitting can be distinguished from the non-micropitted surface on the tooth root due to its texture changes in this zone (red arrow in the magnification frame) . Scratches can be observed on the tip (blue arrow), they are due to some localized scuffing that may occur at high loading stages.

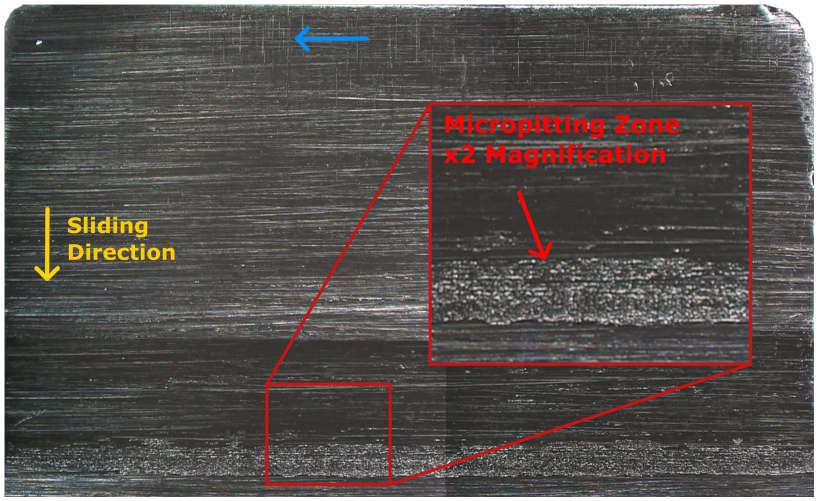

Figure 8: Compiled picture from the wheel tooth surface at stage 3 showing micropitting (red arrow) and scuffing (blue arrow)

The micropitted surface is delimited on the picture and the surface area ratio is estimated as in [24]. The Figure 9 shows the measured surfaces from step 0 to 3b on both the pinion and the wheel.

These two images show that micropitted surface increases from Step 2 to Step 3b at a regular rate. The numerical analysis of these observations reveals that micropitted surface reaches a ratio near 10% (see Figure 10).

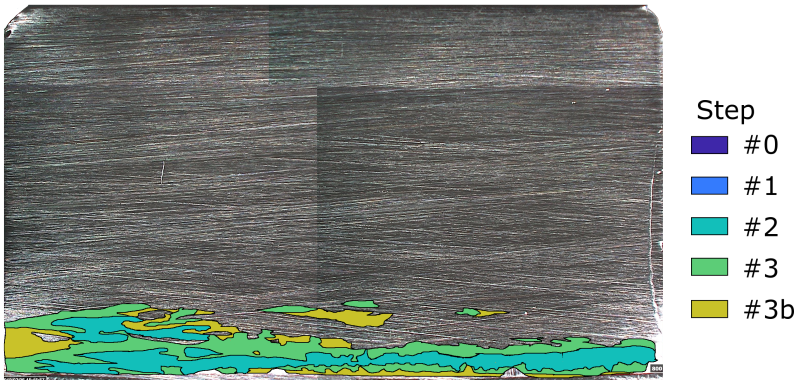

(a) Pinion

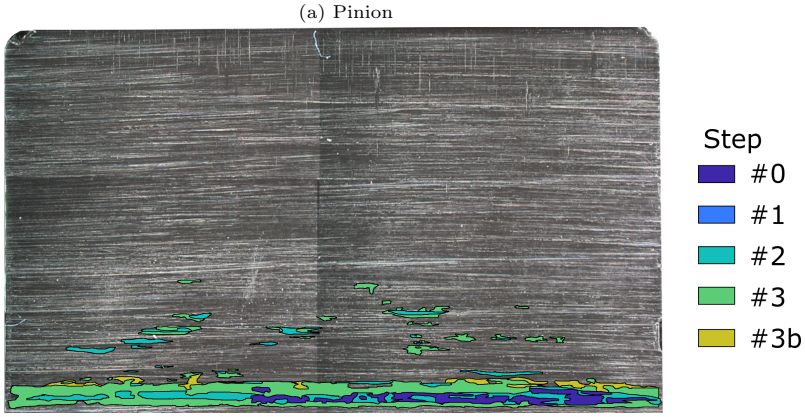

(b) Wheel

Figure 9: Cumulative micropitted surface after step 3b

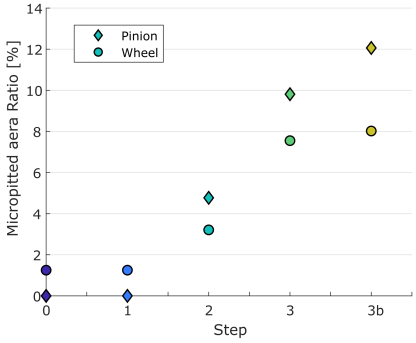

Figure 10: Evolution of the micropitted area ratio

4.3. Correlation between power losses and surface evolution

The measured micropitted area ratio is not sufficient to explain power losses variation. As an example, the decrease of the power losses between step 0 and step 1 cannot be described only by this parameter. Indeed, micropitted area ratio does not change between these two steps.

To be able to find a correlation between micropitting and power losses, it is necessary to investigate surface roughness variation both inside and outside the micropitted zone.

Surfaces are measured using an optical interferometer near tip, pitch and root of gear tooth. Each measured surface represents a $0.9mm \times 1mm$ rectangle. Surface measurements allow to visualize the surface aspect modifications in the densely micropitted zone as shown in Figure 11a and 11b. In these areas, surface aspect is totally modified. Roughness aspect from gear machining is substituted by micropitting. S_q and S_{dq} surface features are reported in Figure 12.

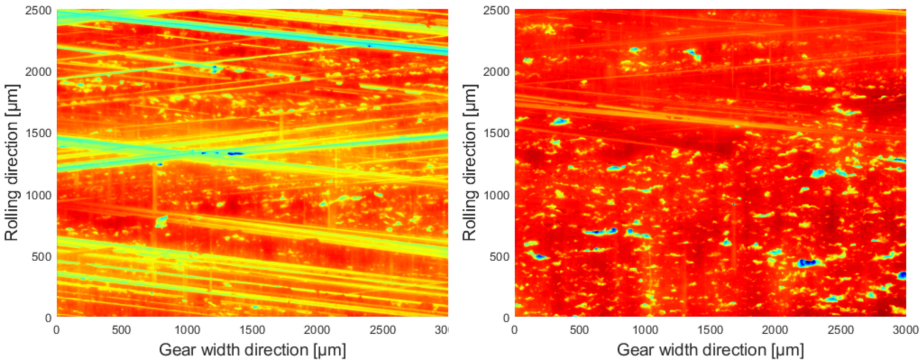

(a) Step 0 (b) Step 3

Figure 11: Surface evolution between step 0 and step 3 at the pinion root

Surface measurements are then computed to estimate surface roughness parameters after each steps and according to the position along the teeth. Figure 12 presents these estimated surface features for one of the pinion teeth.

These figures show that, depending on the location on gear tooth, there is not a single variation tendency for surface features. Near root, roughness tends

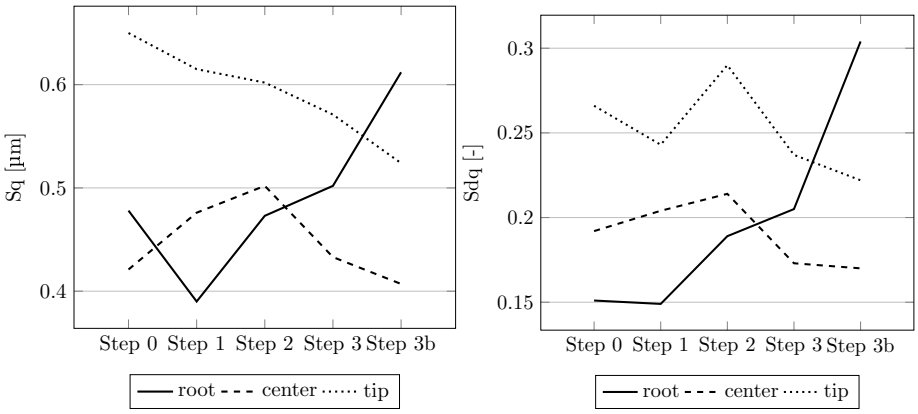

(a) Sq [µm] (b) Sdq [-]

Figure 12: Surface features evolution between step 0 and step 3b for the pinion

to increase whereas it decreases near the tip and center. Near root, micropitting growth could explain this progressive increase.

The evolutions of the surface roughness are consistent with what was observed in the literature. Micropitting tends to develop near the gear root [32, 8] and wear tends to reduce roughness by shaving its tip [33]. It leads to in a competition between the two phenomena [34]. Their influence on roughness may change according to the parameter and the measurement method [24].

If power loss variations are supposed to be related to the friction coefficient ones, it is important to underline that this coefficient changes according to contact speed, loading, lubricant properties and roughness of both surfaces at the point of contact [35]. As speed and loading are identical between each test, and as lubricant temperature is controlled, only surfaces change during the tests. To estimate the average influence of surface roughness modifications during meshing, equivalent surface roughness should be estimated according to surfaces in contact and position along the line of action. As measured power losses and temperatures are not sensitive to instantaneous modification of friction coefficient, the equivalent roughness features are averaged along the line of action to be compared with these measurements.

It is possible to separate three contact zones according to the contact position

during meshing, as presented in Figure 13. In zone a and e, one micropitted surface (pinion or wheel root) is in contact with another surface that does not present any micropitting (pinion or wheel tip). In zone b and d, no micropitting is observed, equivalent surface is estimated with either wheel root and pinion tip or wheel tip and pinion root. In zone c, both pinion and wheel center surfaces interact.

Delimitation between zone e and d or a and b depends on micropitted surface ratio. Between zone b and c or d and c, it depends on the number of teeth in contact estimated from gear geometry [36]: One pair of tooth is in contact in zone C, two pairs of tooth are in contact Zone a,b,d and e)

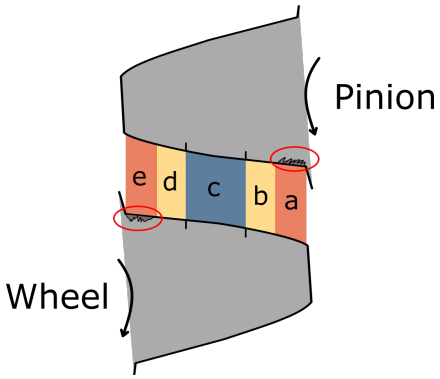

Figure 13: Surfaces interactions during meshing

In the above mentioned zones, equivalent roughness can be estimated from surface features of both surfaces in contact along the line of action, as shown in Equation 4 and 5 [37].

$$S_{q,Eq} = \sqrt{{S_{q,1}}^2 + {S_{q,2}}^2} \tag{4}$$

$$S_{dq,Eq} = \sqrt{{S_{dq,1}}^2 + {S_{dq,2}}^2} \tag{5}$$

For example, in zone e, at step 3, the equivalent quadratic roughness in the

micropitted zone is estimated as expressed in Equation 6:

$$S_{q,Eq,zone,a} = \sqrt{{S_{q,Pinion,root}}^2 + {S_{q,Wheel,tip}}^2} \tag{6}$$

The same approach is applied for all steps along the line of action. Then the average roughness parameters estimated for each step are reported in Figure 14.

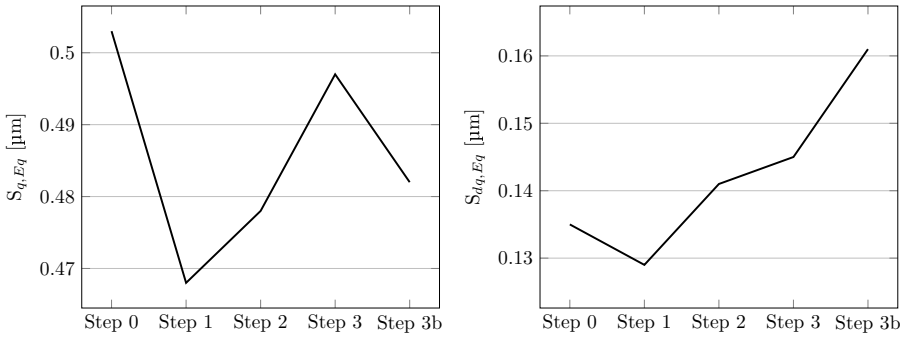

(a) Sq [µm] (b) Sdq [-]

Figure 14: Equivalent surface features evolution along the line of action between steps

From the equivalent quadratic roughness and oil properties it is possible to estimate the Λ ratio, as defined by Tallian [11], (see Figure 15). Values given in the figure show that contact in the gear is characterised by mixed lubrication regime.

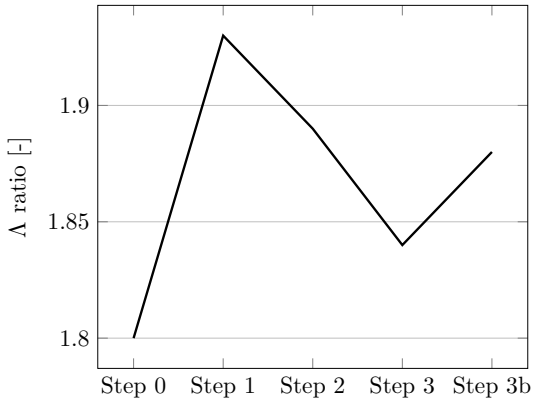

Figure 15: Λ ratio evolution between step 0 and step 3b

With this approach, the variations of the computed surface features are consistent with power losses from step 0 to step 3. The two tendencies associated with power losses measurement also appears on average surface features: decrease between Steps 0 and 1, and increase between Steps 1 and 3. At step 3b, the two surface parameters behave differently: Sq tends to decrease whereas Sdq tends to increase.

These tendencies, can be explained knowing that favourable conditions for the development of micropitting are similar to the ones for wear [11, 38]. Therefore, both these phenomena can occur simultaneously on the surfaces and compete with each other: wear tends to reduce surface roughness by degrading machining marks whereas micropitting tends to increase this roughness by adding small pits on the surface. This is well illustrated by Figure 11b where machining marks can not be observed any more because of dense micropitting.

Between Steps 0 and 1, fatigue operating conditions do not generate micropitting growth. Yet the surface is still subject to wear. As a result, the equivalent surface roughness and power losses decrease. Between Steps 1 and 3, micropitted area increases significantly. This one generates an increase of the average surface roughness consistent with power losses. At step 3b, variations are more complex to describe. Equivalent surface features may be more significantly influenced by the modification of the surface aspect due to the increase of the micropitted area. In the associated zone, surface changes from an oriented surface roughness due to gear machining (as shown in Figure 11a) to a flat surface with micropitting (as shown in Figure 11b).

5. Temperature measurements and analyses

As torque measurements are not frequently used in industrial applications, it is important to analyse if temperature could be a good indicator instead of power losses. Indeed, temperature is easier to measure and is related to the level of power losses as underlined by Equation 3.

From a test to another, room temperature may vary slightly. This variation

involves a temperature offset that must be taken into account to accurately compare temperatures. Gearbox temperature is analysed regarding ambient air temperatures as shown by equation 7.

$$T_{Rel}(Oil) = T(Oil) - T(Air) \tag{7}$$

Similarly to power losses, temperatures are averaged using 10 minutes of measurements from the 110th minute of the test. The average air temperature changes from a test to another between 42.4 °C and 40.0 °C which leads to in an absolute oil temperature around 70 °C.

Finally the average relative oil temperature is plotted on figure 16. Temperature changes in a range of 3 °C. This variation underlines temperature sensitivity to power loss modifications and so to surface roughness evolutions due to micropitting.

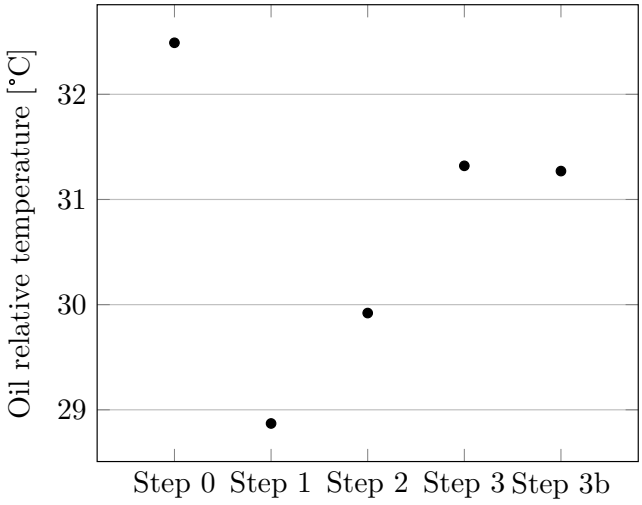

Figure 16: Evolution of the measured average temperature during characterization tests

The correlation between power losses and oil temperature can be drawn. As shown by Figure 7 and 16 both temperature and power losses follow the same trend between steps. As suggested by the theoretical approach, Figure 17 clearly underlines the linearity between power losses and temperature variations.

As power losses are experimentally correlated to surface evolutions, it implies that oil temperature, by itself, is also a good indicator of these surface feature evolutions.

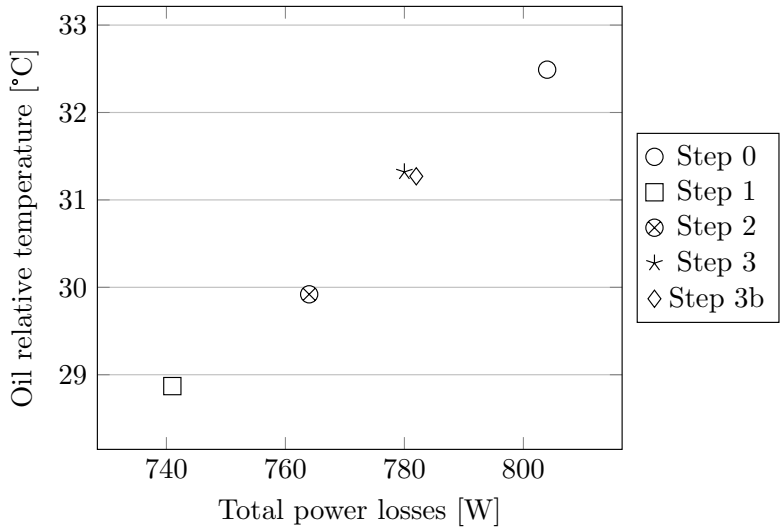

Figure 17: Correlation between temperatures and power losses measured across steps

Tests also show that it is important to consider indicator variations over time. Indeed, in these experiments, temperature decreases to a lower value that the initial one (between steps 0 and 1) before increasing to a new value (step 3). Yet, temperatures measured on steps 3 and 3b are lower than the initial one. As a consequence, try to identify the presence of micropitting at step 3 would not be possible without knowing temperature previously reduced at step 1.

6. Conclusions on the effect of micropitting on friction and power losses and temperatures

In a previous paper (part 1 of the study [18]) the authors have shown that micropitting has a significant influence on friction coefficient. This paper presents an extension of these results to a complete gear train. An experimental approach to analyse the influence of micropitting on gearbox power losses is presented. To this end, a back-to-back FZG test rig was used.

Several experimental results were presented in this paper. They showed that micropitting, even for a limited amount, can have an influence on power losses of a complete geared system.

The measurement of the roughness features along with the amount of micropitted surfaces allowed to estimate equivalent surface roughness parameters of the contacts. These parameters follow the same trends than power losses, showing a correlation between micropitting and power losses.

Micropitting also induced measurable variation of oil temperature. This observation supports the interest of temperature measurements in order to detect evolution of contact surface in gears. Furthermore, the good correlation observed with power losses tends to show the reliability of temperature measurements to assess power loss modifications -and so friction coefficient- in a geared mechanical system.

Yet, in the perspective of health monitoring, the defect magnitude estimation (i.e. the micropitted area) based on temperature measurements remains a complex task. It is not possible at this point to propose a law that could directly link the temperature variations to the micropitting severity. Being able to diagnose precisely geared system health based on temperature measurements is still a future work to be conducted.

Nomenclature

α	Pressure angle [deg]
ε_α	Contact ratio [-]
A	Area [m ^{2}]
a	Operating Center distance [mm]
b	Tooth width [mm]
f	Average friction coefficient [-]
H_v	Tooth power loss geometry parameter [-]

	k	Heat exchange coefficient [W/m ^{2} °K]
	m	Module [mm]
	P	Power [W]
	S_{dq}	Surface average quadratic roughness slope [-]
	S_q	Surface average quadratic roughness amplitude [m]
	T	Temperature [°C]
	X_i	Profile shift modification [-]
	Z_i	Number of teeth [-]

References

[1] D. Wang, K. L. Tsui, Q. Miao, Prognostics and Health Management: A Review of Vibration Based Bearing and Gear Health Indicators, IEEE Access 6 (2017) 665–676. doi:10.1109/ACCESS.2017.2774261.

[2] T. Wang, Q. Han, F. Chu, Z. Feng, Vibration based condition monitoring and fault diagnosis of wind turbine planetary gearbox: A review, Mechanical Systems and Signal Processing 126 (2019) 662–685. doi:10.1016/j.ymssp.2019.02.051.
URL https://doi.org/10.1016/j.ymssp.2019.02.051

[3] D. Remond, Practical performances of high-speed measurement of gear transmission error or torsional vibrations with optical encoders, Measurement Science and Technology 9 (3) (1998) 347–353. doi:10.1088/0957-0233/9/3/006.

[4] J. B. Roylance, J. A. Williams, R. Dwyer-Joyce, Wear debris and associated wear phenomena—fundamental research and practice, Proceedings of the Institution of Mechanical Engineers. Part J, Journal of engineering tribology 214 (1) (2000) 79–105. doi:10.1243/1350650001543025.

[5] A. R. Mohanty, C. Kar, Fault detection in a multistage gearbox by demodulation of motor current waveform, IEEE Transactions on Industrial Electronics 53 (4) (2006) 1285–1297. doi:10.1109/TIE.2006.878303.

[6] T. Touret, C. Changenet, F. Ville, M. Lalmi, S. Becquerelle, On the use of temperature for online condition monitoring of geared systems – A review, Mechanical Systems and Signal Processing 101 (2018) 197–210. doi:10.1016/j.ymssp.2017.07.044.

[7] A. V. Olver, The Mechanism of Rolling Contact Fatigue: An Update, Proceedings of the Institution of Mechanical Engineers, Part J: Journal of Engineering Tribology 219 (5) (2005) 313–330. doi:10.1243/135065005X9808.

[8] R. Errichello, Morphology of Micropitting, Gear technology (December) (2012) 74–81.

[9] F. Antoine, J.-m. Besson, D. Stress, Simplified modellization of gear micropitting 216 (October) (2002) 291–303.

[10] J. A. Brandao, R. Martins, J. H. Seabra, M. J. Castro, Surface damage prediction during an FZG gear micropitting test, Proceedings of the Institution of Mechanical Engineers, Part J: Journal of Engineering Tribology 226 (12) (2012) 1051–1073. doi:10.1177/1350650112461879.

[11] T. E. Tallian, E. F. Brady, J. I. Mccool, L. B. Sibley, Lubricant Film Thickness and Wear in Rolling Point Contact, A S L E Transactions 8 (4) (1965) 411–424. doi:https://doi.org/10.1080/05698196508972111.

[12] P. Rabaso, T. Gauthier, M. Diaby, F. Ville, Rolling Contact Fatigue: Experimental Study of the Influence of Sliding, Load, and Material Properties on the Resistance to Micropitting of Steel Discs, Tribology Transactions 56 (2) (2013) 203–214. doi:10.1080/10402004.2012.737504.

[13] A. Fabre, L. Barrallier, M. Desvignes, H. P. Evans, M. P. Alanou, Micro-geometrical influences on micropitting fatigue damage: multi-scale analy-

sis, Proceedings of the Institution of Mechanical Engineers, Part J: Journal of Engineering Tribology 225 (6) (2011) 419–427. doi:10.1177/1350650110396980.

[14] M. Le, F. Ville, X. Kleber, J.-Y. Buffière, J. Cavoret, M.-C. Sainte-Catherine, L. Briancon, Rolling contact fatigue crack propagation in nitrided alloyed steels, Proceedings of the Institution of Mechanical Engineers, Part J: Journal of Engineering Tribology 0 (0) (2017). doi:10.1177/1350650117717824.

[15] E. Bossy, J. P. Noyel, X. Kleber, F. Ville, C. Sidoroff, S. Thibault, Competition between surface and subsurface rolling contact fatigue failures of nitrided parts: A Dang Van approach, Tribology International 140 (July) (2019). doi:10.1016/j.triboint.2019.105888.

[16] E. Lainé, A. V. Olver, M. F. Lekstrom, B. A. Shollock, T. A. Beveridge, D. Y. Hua, The effect of a friction modifier additive on micropitting, Tribology Transactions 52 (4) (2009) 526–533. doi:10.1080/10402000902745507.

[17] E. de la Guerra Ochoa, J. E. Otero, E. Chacón Tanarro, J. M. Munoz-Guijosa, B. del Río López, C. A. Cordero, Analysis of the effect of different types of additives added to a low viscosity polyalphaolefin base on micropitting, Wear 322-323 (2015) 238–250. doi:10.1016/j.wear.2014.11.014.

[18] T. Touret, C. Changenet, F. Ville, J. Cavoret, V. Abousleiman, Experimental investigations on the effect of micropitting on friction – Part 1, Tribology International (mar 2019). doi:10.1016/j.triboint.2019.03.036.

[19] E. u. K. e.V Deutsche Wissenschaftliche Gesellschaft für Erdöl, Short Test Procedure for the investigation of the micropitting load capacityof gear lubricants, DGMK Information sheet 2002 (August) (2002).

[20] F. information sheet, FVA 54/7 Test procedure for the investigation of the micropitting capacity of gear lubricant (1993).

[21] R. Martins, J. Seabra, L. Magalhães, Austempered ductile iron (ADI) gears: Power loss, pitting and micropitting, Wear 264 (9-10) (2008) 838–849. doi:10.1016/j.wear.2007.05.007.

[22] N. F. R. Cardoso, R. C. Martins, J. H. O. Seabra, A. Igartua, J. C. Rodríguez, R. Luther, Micropitting performance of nitrided steel gears lubricated with mineral and ester oils, Tribology International 42 (1) (2009) 77–87. doi:10.1016/j.triboint.2008.05.010.

[23] N. F. R. Cardoso, R. C. Martins, J. H. O. Seabra, Micropitting of carburized gears lubricated with biodegradable low-toxicity oils, Proceedings of the Institution of Mechanical Engineers, Part J: Journal of Engineering Tribology 223 (3) (2009) 481–495. doi:10.1243/13506501JET495.

[24] R. Martins, C. Locatelli, J. Seabra, Evolution of tooth flank roughness during gear micropitting tests, Industrial Lubrication and Tribology 63 (1) (2011) 34–45. doi:10.1108/00368791111101821.

[25] N. Ludivion, ISO/TS 6336-4 Calcul de la capacité de charge au grippage des engrenages cylindriques, coniques et hypoïdes, Tech. rep. (2016).

[26] C. M. C. G. Fernandes, P. M. T. Marques, R. C. Martins, J. H. O. Seabra, Tribology International Gearbox power loss . Part II : Friction losses in gears, Tribiology International 88 (2015) 309–316. doi:10.1016/j.triboint.2014.12.004.

[27] Y. Diab, F. Ville, P. Velex, Investigations on power losses in high-speed gears, Proceedings of the Institution of Mechanical Engineers, Part J: Journal of Engineering Tribology 220 (3) (2006) 191–198. doi:10.1243/13506501JET136.

[28] ISO, Gears - Thermal capacity Part 2 : Thermal load-carrying capacity, Tech. rep. (2001).

[29] B. Kelley, A. J. Lemanski, Lubrication of involute gearing, Proceedings of the Institution of Mechanical Engineers 182 (1) (1967) 173–184. doi:https://doi.org/10.1243/PIME_CONF_1967_182_016_02.

[30] Y. Diab, F. Ville, P. Velex, Prediction of Power Losses Due to Tooth Friction in Gears, Tribology Transactions 49 (2) (2006) 260–270. doi:10.1080/05698190600614874.
URL http://www.tandfonline.com/doi/abs/10.1080/05698190600614874

[31] C. Changenet, X. Oviedo-Marlot, P. Velex, Power Loss Predictions in Geared Transmissions Using Thermal Networks-Applications to a Six-Speed Manual Gearbox, Journal of Mechanical Design 128 (3) (2006) 618. doi:10.1115/1.2181601.

[32] P. W. Predki, K. Nazifi, G. Lützig, Micropitting of Big Gearboxes : Influence of Flank Modification and Surface Roughness, in: VDI, no. May, 2011.

[33] G. Morales-Espejel, V. Brizmer, E. Piras, Roughness evolution in mixed lubrication condition due to mild wear, Proceedings of the Institution of Mechanical Engineers, Part J: Journal of Engineering Tribology 229 (11) (2015) 1330–1346. doi:10.1177/1350650115577404.
URL http://pij.sagepub.com/lookup/doi/10.1177/1350650115577404

[34] G. E. Morales-Espejel, P. Rycerz, A. Kadiric, Prediction of micropitting damage in gear teeth contacts considering the concurrent effects of surface fatigue and mild wear, Wear 398-399 (November 2017) (2018) 99–115. doi:10.1016/j.wear.2017.11.016.
URL https://doi.org/10.1016/j.wear.2017.11.016

[35] G. H. Benedict, B. W. Kelley, Instantaneous Coefficients of Gear Tooth Friction, A S L E Transactions 4 (1) (1961) 59–70. doi:10.1080/05698196108972420.

[36] E. Buckingham, Analytical Mechanics of Gears, 2002.

[37] J. I. McCool, Comparison of models for the contact of rough surfaces, Wear 107 (1) (1986) 37–60. doi:10.1016/0043-1648(86)90045-1.

[38] E. Lainé, A. V. Olver, T. A. Beveridge, Effect of lubricants on micropitting and wear, Tribology International 41 (11) (2008) 1049–1055. doi:10.1016/j.triboint.2008.03.016.